Taguchi Optimisation of Friction Stir Welding Parameters for Pure Aluminium under Different Backing Conditions

Sufian Raja [1,2], Aleksey Yushin [1,b *], Chunlei He [2,c *], Pavlo Goncharov [1], Fomichev Evgenii [1], Vadim Verkhorubov [1], Huan Miao [3]

RESEARCH ARTICLE

ARTICLE INFO

Keywords:

Backing condition; Friction stir welding; Joint efficiency; Pure aluminium; Taguchi method

Article History

*Received:*24 October 2025
*Revised:*19 February 2026
*Accepted:*28 February 2026
Published:

ABSTRACT

Friction stir welding (FSW) of pure aluminium is highly sensitive to the backing condition because the backing plate not only supports the workpiece against downward forging but also governs heat extraction from the weld zone. This study optimized the FSW parameters for 6-mm pure aluminium under three backing conditions: aluminium, mild steel, and an insulating fly-ash bed, and evaluated their effects on tensile strength, joint efficiency, hardness, fracture morphology, and phase stability. Butt joints were produced on a vertical milling machine using a low-cost dedicated fixture. A Taguchi L9 orthogonal array was employed to examine tool rotational speed, welding speed, and tool geometry (straight cylindrical, triangular, and straight square), followed by ANOVA and regression-based optimisation. The base metal showed 180.793 MPa ultimate tensile strength, 34.3% elongation, and 75.2 HRB hardness. The aluminium backing condition yielded 93.20-113.41 MPa and 51.55-62.72% joint efficiency, while mild steel gave 72.43-139.10 MPa and 40.06-76.93%. The fly-ash bed produced the best performance, achieving 107.10-165.78 MPa and 59.23-91.69% joint efficiency, with a maximum tensile strength of 165.78 MPa. Hardness was highest under aluminium backing and remained closer to the base metal under fly ash. Fractography showed tunnel defects, voids, and coarse dimples in the aluminium condition, fewer severe features in mild steel, and abundant fine dimples indicative of ductile fracture in the fly-ash condition. XRD showed no additional peaks, confirming the absence of foreign material transfer into the nugget. These findings show that backing condition is a key optimisation variable and that fly ash is an effective low-cost insulating backing medium for improving weld performance in pure aluminium FSW.

1. Introduction

Aluminium and its alloys continue to be among the most important structural materials for lightweight engineering because they provide a useful combination of low density, good corrosion resistance, and adequate specific strength. These properties make them well-suited to transportation, marine, aerospace, and general fabrication applications (Bharti et al., 2023; Feddal et al., 2025). In these sectors, however, the structural usefulness of aluminium depends not only on the base material itself but also on the soundness of the joints used to connect plates, extrusions, and formed parts. For this reason, friction stir welding (FSW) continues to attract strong academic and industrial attention as a solid-state joining technique that avoids bulk melting and can therefore reduce many of the problems associated with conventional fusion welding, such assolidification-related defects, high distortion, and inconsistent weld quality (Heidarzadeh et al., 2021; Isa et al., 2021; Lunetto et al., 2025; Raja et al., 2016).

1 Daou (Shaoxing) Technology Co., Ltd, Room 6048, Building 6, East Zone, Keqiao International Park, No.199 Chuangyi Road, Keqiao District, Shaoxing City, Zhejiang Province, China
2 Tianjin Key Laboratory of Equipment Design and Manufacturing Technology, Tianjin University, Tianjin 30054, China
3 College of Materials Engineering, North China Institute of Aerospace Engineering, Langfang, 065000, China.
Corresponding authors:

Recent review papers confirm that FSW remains one of the most intensively studied solid-state joining processes for aluminium systems, not only for standard butt and lap joints but also for more complex industrial geometries and dissimilar material combinations. At the same time, post-weld property tailoring and process modelling are receiving increasing research interest (Amini et al., 2022; Choi et al., 2025; Habba & Ahmed, 2025; Raja et al., 2020).

Despite these advantages, FSW remains highly sensitive to process control because joint formation depends on a complex interaction between frictional heat generation, plastic deformation, material flow, and final consolidation beneath the shoulder and around the pin (Heidarzadeh et al., 2021; Raja et al., 2024; Yamani et al., 2022). As a result, weld quality is strongly affected by the main process parameters, especially tool rotational speed, welding speed, and tool geometry. Many recent studies have therefore focused on the statistical and computational optimisation of FSW conditions for aluminium alloys, using approaches such as Taguchi design, grey relational analysis, response surface methodology, artificial intelligence, and hybrid predictive models to identify parameter combinations that maximise tensile strength, hardness, or overall joint efficiency (Abdelhady et al., 2024; Ahmed et al., 2022; Asmare et al., 2020; Clark & Ragai, 2025; Kubit et al., 2022; Manjunatha et al., 2025; Myśliwiec et al., 2024; Soto-

Diaz et al., 2025). These studies consistently show that unsuitable parameter combinations can lead either to insufficient heat input and incomplete consolidation or to excessive heat input and mechanical softening, both of which reduce weld performance (Abdelhady et al., 2024; Ahmed et al., 2022; Kubit et al., 2022; Mohd Jamil et al., 2024; Raja et al., 2022).

A substantial part of the recent literature has concentrated on aluminium alloys such as AA6061, AA2024, AA5052, AA5083, and AA5754, because these alloys are widely used in engineering and because their responses to friction stir welding are strongly shaped by thermal history (Feddal et al., 2025; Lunetto et al., 2025). In AA6061 and related systems, the combined effects of tool profile, rotational speed, feed rate, and thermal cycle have been linked to tensile performance, hardness variation, fracture morphology, and defect formation (Abdollahzadeh et al., 2021; Wahjudi et al., 2024). Studies on conventional, bobbin-tool, friction stir spot, and modified-joint configurations have shown that tensile strength and fracture mode are highly sensitive to the degree of consolidation and local thermal exposure, while hardness distributions are likewise affected by weld geometry and process condition (Tinguery et al., 2023; Tiwan et al., 2023; Yacout et al., 2025). Recent work has also continued to use fractography as an essential validation tool for distinguishing defect-assisted fracture from more ductile failure modes in aluminium FSW joints (Abdollahzadeh et al., 2021; Wahjudi et al., 2024).

Beyond the commonly discussed tool and travel parameters, an equally important but often underemphasised factor is the thermal boundary condition imposed by the backing system. In the present study, the term backing condition refers to the material or medium placed beneath the workpiece to provide mechanical support during welding while simultaneously governing heat extraction from the lower side of the joint. Accordingly, the backing system acts both as a structural support and as a thermal pathway, and can therefore alter peak temperature, cooling rate, through-thickness temperature gradient, and the stability of plasticised material flow. The significance of this issue has become more visible in recent years. Studies on aluminium alloys have shown that changes in backing plate material or thermal boundary condition can modify microstructure, hardness, strength, and defect susceptibility (Das et al., 2024; Mondal et al., 2024; Raja et al., 2021). High-conductivity support conditions may intensify heat loss and thereby increase the risk of insufficient consolidation, whereas thermally resistant or differently configured support conditions can retain heat and alter weld behaviour. Recent work on backing-plate effects, dual-backing concepts, and large-thickness thermal boundary control confirms that backing is not merely a passive fixture detail but a variable with direct metallurgical and mechanical consequences (Acharya et al., 2024; Al-Allaq et al., 2024; Ambrosio et al., 2024; Das et al., 2024; Verma et al., 2025).

For heat-treatable alloys such as AA6061, this thermal-boundary issue is especially important because the weld thermal cycle influences precipitate evolution, local softening, hardness minima, and ultimately failure location (Zhou et al., 2024). Recent studies have shown that mechanical performance in friction stir-welded AA6061 joints is closely linked to hardness evolution and local fracture behaviour, and that the interpretation of tensile data becomes stronger when supported by hardness mapping and fractographic analysis (Abdelhady et al., 2024; Wahjudi et al., 2024; Yacout et al., 2025).

However, although recent optimisation and property studies on aluminium alloys are extensive, several limitations remain when viewed from the perspective of a practical, mechanically focused manuscript. First, most recent studies deal with alloy-specific systems such as AA6061, AA2024, AA5754, AA5052, or composite-containing aluminium systems, while comparatively fewer works isolate the effect of backing condition in a simpler pure-aluminium system where precipitation-related complexity is absent.

Second, many optimisation studies treat the backing arrangement as fixed and concentrate primarily on tool geometry and speed variables (Abdelhady et al., 2024; Ahmed et al., 2022; Kubit et al., 2022). Third, while advanced modelling and machine-learning methods are increasingly reported, there remains clear value in experimentally grounded, low-cost, shop-floor-compatible studies that combine parameter optimisation with direct mechanical verification, particularly for conditions such as conventional vertical milling machines (Manjunatha et al., 2025; Myśliwiec et al., 2024; Soto-Diaz et al., 2025). In this context, a controlled comparison among conductive and insulating backing conditions remains both scientifically relevant and industrially useful (Feddal et al., 2025; Yacout et al., 2025).

The present study was therefore designed to investigate friction stir welding of 6-mm pure aluminium under different backing conditions and to optimise the process parameters for maximum tensile strength using a Taguchi L9 orthogonal array. Unlike studies centred on extensive metallurgical characterisation, the present work is positioned as a process-optimisation and weld-performance study in which three backing conditions are compared under the same experimental framework. The effects of rotational speed, welding speed, and tool geometry are evaluated in relation to tensile strength and joint efficiency, while hardness mapping and SEM fractography are used to support the interpretation of thermal and failure responses.

X-ray diffraction is additionally employed as a conservative verification step to confirm that the backing condition does not introduce detectable foreign material into the weld zone. In this way, the study seeks to clarify whether backing condition can be treated as a practical optimisation variable in pure-aluminium FSW and whether an insulating backing medium can provide a low-cost route for improving weld performance.

2. Materials and Methods

Commercially available pure rolled aluminium was used as the base material in the present investigation because it allows the friction stir welding response to be examined without the added complexity of alloying-element effects. The rolled plates were cut into 100 × 70 × 6 mm coupons and welded in a butt-joint configuration. EDX analysis of the parent plate confirmed that the workpiece was aluminium, and the base metal exhibited an ultimate tensile strength of 180.793 MPa, elongation of 34.3%, and hardness of 75.2 HRB, as shown in Tables 1 and 2. Table 1 reports the experimentally measured EDX composition of the parent plate, while Table 2 reports the experimentally measured base-metal tensile and Rockwell hardness values obtained in this study. Tensile testing was conducted according to ASTM E8/E8M, and hardness measurement was performed using the Rockwell method in accordance with ASTM E18.

Table 1. Chemical composition of the base material

Element	Weight (%)	Atomic (%)
Al	100.00	100.00

Table 2. Mechanical properties of the base material

Properties	Value
Ultimate tensile strength (MPa)	180.793
Elongation (%)	34.3
Hardness (HRB)	75.2

Since the welding trials were carried out on a vertical milling machine, the development of a reliable fixture was a necessary part of the experimental design. A dedicated fixture was therefore designed and fabricated in-house from mild steel to provide proper alignment, rigid support, and resistance against the unbalanced forces generated during welding, as shown in Figure 1. The schematic of the fixture is shown in Figure 1 (a) and Figure 1 (b). The fabricated fixture assembly is shown in Figure 1 (c). The FSW experiments were performed on a vertical milling machine with 8 spindle-speed steps (250-4500 rpm), manual table feed, and 1 hp motor power. The tool was mounted using a suitable collet, and because the machine did not provide independent tilt-angle adjustment, the process variables were selected within the available machine and setup limitations.

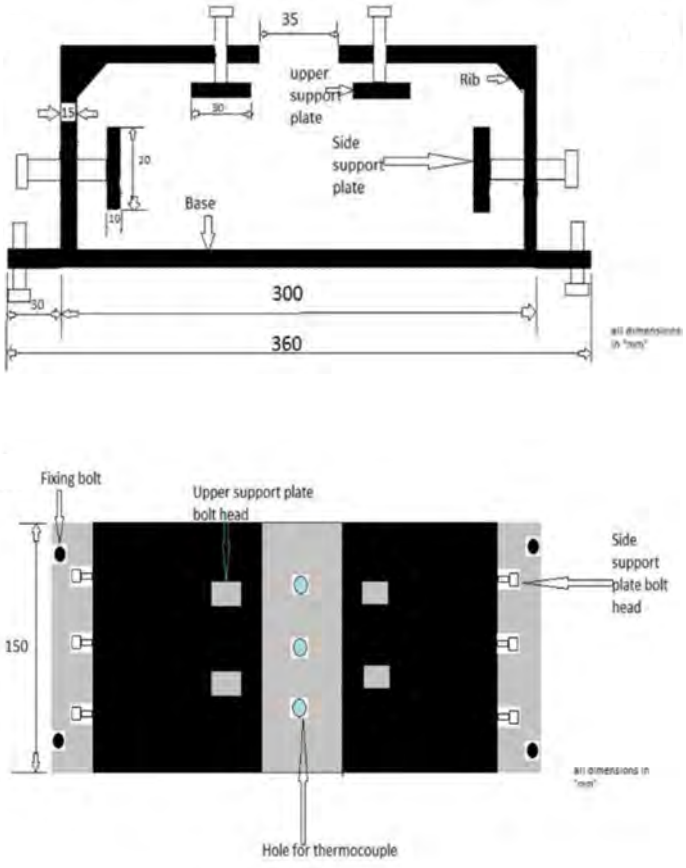

Figure 1. (a) Front view of developed fixture, (b) top view of developed fixture, and (c) complete fixture assembly

The welding tools were fabricated from stainless steel (Grade 310) because of its high-temperature capability and adequate ductility under the combined torque and vertical pressure of the FSW process. Grade 310 stainless steel was selected not only for strength and hot-hardness retention during FSW, but also because its thermal conductivity is much lower than that of pure aluminium. As a result, the tool itself did not behave as a major heat sink relative to the aluminium backing; instead, it helped retain frictional heat locally around the shoulder–pin region, whereas the backing condition primarily governed the through-thickness heat extraction from the weld (Das et al., 2024; Park et al., 2020). Three tool-pin geometries were prepared: straight cylindrical (SC), triangular (TL), and straight square (SS). The tools were machined initially from a 22 mm diameter stainless-steel bar. The straight cylindrical tool was produced directly by lathe machining, whereas the square and triangular profiles were prepared by first machining a cylindrical pin and then forming the required profile on a milling machine. The fixed tool dimensions used in the study were a 5 mm probe length, 6 mm probe diameter/side length, and 18 mm shoulder diameter, as shown in Figure 2 and tabulated in Table 3.

Table 3. Tool geometry used in FSW of Al

Parameter	Value
Tool material	Stainless steel (Grade 310)
Tool profiles	Straight cylindrical (SC) Triangular (TL) Straight square (SS)
Probe length	5 mm
Probe diameter/ side length	6 mm
Shoulder diameter	18 mm

To examine the effect of thermal boundary conditions on weld performance, three distinct backing conditions were used. In the aluminium condition, the bottom back plate, top support, and side support were made of pure aluminium, as shown in Figure 3 (a). In the mild-steel condition, the supporting enclosure was made of mild steel, as shown in Figure 3(b). In the fly-ash backing condition, a rigid mild-steel box was filled with dry fly ash, and the lower surface of the aluminium plate rested directly on the top surface of the fly-ash bed during welding. Thus, the specimen was mechanically supported by the steel enclosure while the immediate lower interface beneath the plate was a particulate insulating layer rather than a solid metallic back plate, as shown in Figures 3 (c) and (d).

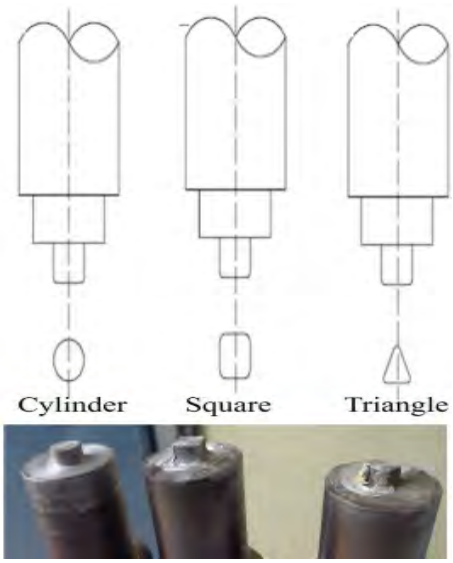

Figure 2. Tool geometry employed in the friction stir welding experiments

In each case, the welded plate was kept in the same condition until cooling to room temperature. The three conditions were selected because they provide a wide variation in thermal conductivity, namely 205–250 W/m·K for pure aluminium, 40–50 W/m·K for mild steel, and 0.15–1.3 W/m·K for fly ash.

Fly ash was selected as the insulating filler because it is a particulate oxide-rich residue with much lower thermal conductivity than the metallic backing materials. Dry fly ashes are reported to exhibit low thermal conductivity, and fly-ash-based materials are widely used in thermal-insulation applications. In the present work, EDX of the fly ash detected C, O, Al, Si, and K as the major elements, confirming that the filler was an oxide-rich particulate medium suitable for use as a thermally resistive backing condition rather than a metallic heat sink, as shown in Figure 4.

The experimental design was based on a Taguchi L9 orthogonal array, selected to evaluate the effects of three major process variables under the constraints of the machine and setup. These variables were tool rotational speed, welding speed, and tool geometry, each examined at three levels. Prior trial welds were carried out to confirm the feasible parameter range, and the L9 array was selected because it allowed the effects of the three factors to be studied with an economically manageable number of runs while satisfying the required degrees of freedom for the design. The three levels considered were 544, 1100, and 1850 rpm for rotational speed; 60, 90, and 120 mm/min for welding speed; and SC, TL, and SS for tool geometry, as shown in Table 4 and Table 5.

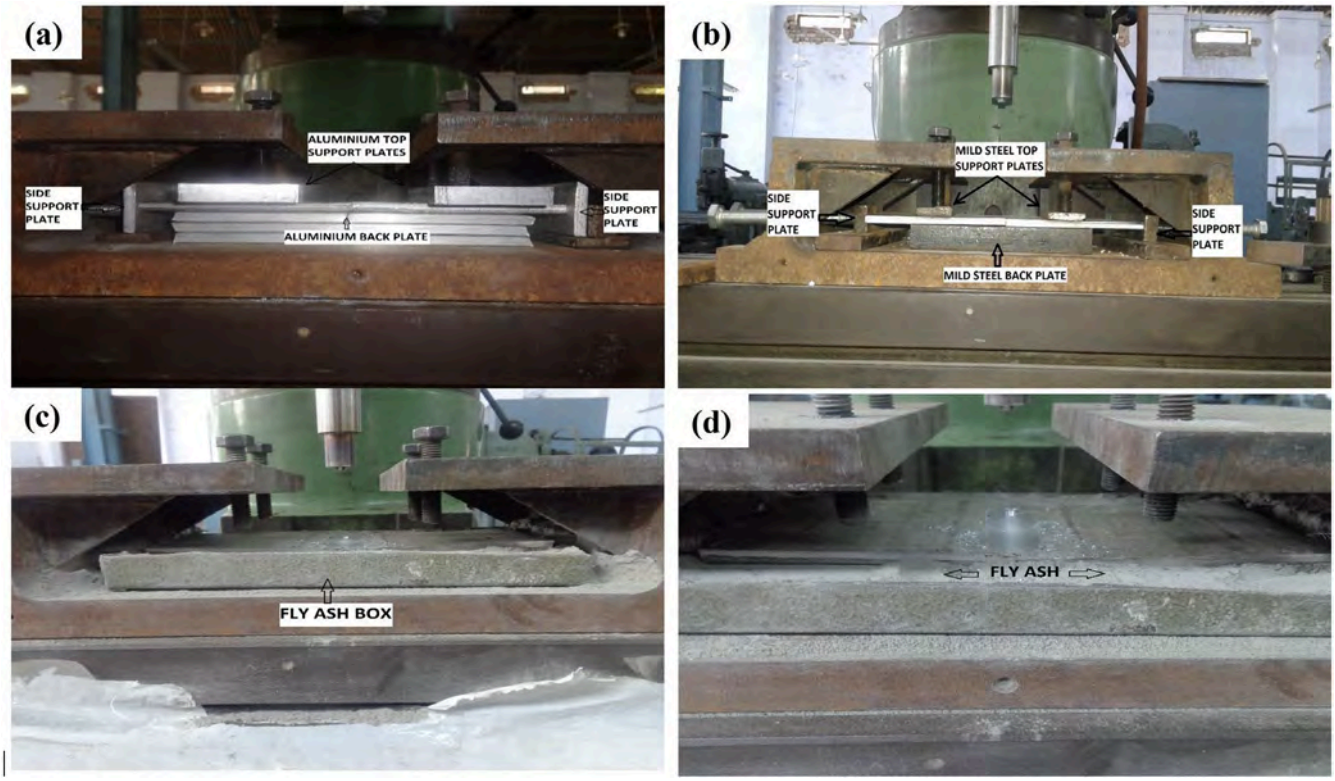

Figure 3. Backing conditions used in the present work: (a) aluminium backing condition setup, (b) mild-steel backing condition setup, (c) fly-ash backing condition showing the plate positioned over the fly-ash-filled steel box during welding,

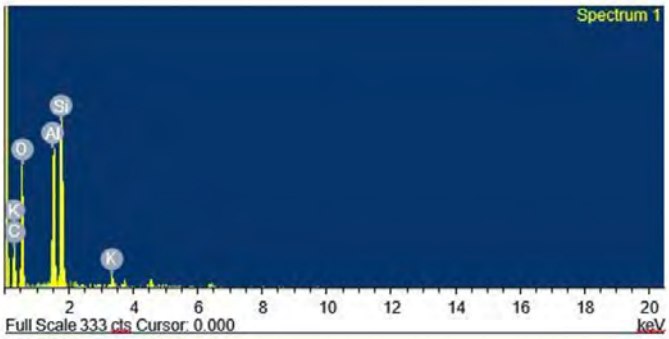

Figure 4. SEM-EDX of fly ash showing different elements

Table 4. Process parameters and levels used in the Taguchi design

Parameter	Level 1	Level 2	Level 3
Tool rotational speed (rpm)	544	1100	1850
Welding speed (mm/min)	60	90	120
Tool geometry	Straight cylinder (SC)	Triangular (TL)	Straight square (SS)

Table 5. L9 orthogonal array used for the welding experiments

Run	Tool rotational speed (rpm)	Welding speed (mm/min)	Tool geometry
1	544	60	SC
2	544	90	TL
3	544	120	SS
4	1100	60	TL
5	1100	90	SS
6	1100	120	SC
7	1850	60	SS
8	1850	90	SC
9	1850	120	TL

After welding, the joints were sectioned and machined into tensile specimens according to ASTM E8 geometry, as depicted in Figure 5 (a). Tensile testing was carried out on a digitally controlled servo-hydraulic dynamic testing machine using a displacement-controlled crosshead speed of 2 mm/min. Weld performance was evaluated primarily through tensile strength and joint efficiency. Joint efficiency was determined with respect to the base-metal tensile strength.

Hardness measurements were performed using a digital Rockwell hardness tester. The hardness values were recorded from the weld centre at 5 mm increments on both the advancing and retreating sides. Measurements were taken at three thickness levels, namely 2 mm, 4 mm, and the bottom/root region, measured from the top surface of the weld shown in Figure 5 (b). This layout allowed the crown-to-root hardness variation to be assessed in addition to the transverse hardness profile across the joint.

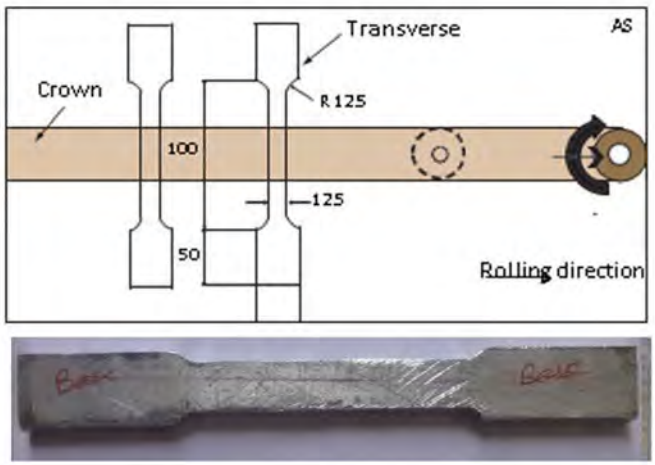

(a)

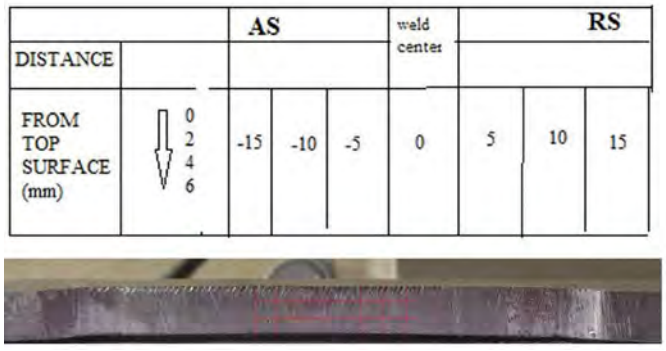

(b)

Figure 5. (a) Standard tensile test specimen (b) hardness-mapping layout

After tensile testing, the fracture surfaces of selected specimens were examined using scanning electron microscopy (SEM) in order to analyse fracture morphology and relate failure mode to weld quality. In addition, X-ray diffraction (XRD) was performed on the base metal and selected welds to examine whether any temperature-related phase changes or unwanted foreign particles were present in the nugget region, particularly in the case of the fly-ash backing condition. For the Taguchi analysis, the tensile-strength data were converted to signal-to-noise ratios using the larger-the-better criterion, and ANOVA was performed to determine the significance of each process parameter.

3. Results

3.1 Weld appearance and macroscopic integrity

A clear difference in weld surface quality was observed among the three backing conditions, as depicted in Fig. 6. Under the aluminium backing condition, the welded specimens showed visible defects, including flash formation and tunnel-type defects, indicating that the weld bead was not fully stable under the high-conductivity backing condition (Figure 6 (a),(b)). In contrast, the mild-steel backing condition produced a smoother weld bead, and records that the major visible defects observed in the aluminium condition were eliminated, as shown in Fig 6(c). The most satisfactory macroscopic appearance was obtained in the fly-ash backing condition, where the welded zone was reported to have a smooth, defect-free, mirror-like surface compared with both metallic backing conditions, Figure 6 (d). These observations provide the first indication that the backing condition strongly influenced heat retention and weld-bead stability during the process.

3.2 Tensile strength and joint efficiency

The base metal used in this work exhibited an ultimate tensile strength of 180.793 MPa, which was taken as the reference for joint-efficiency calculations. Across all experiments, the tensile response was strongly affected by backing condition, and the overall trend showed that joint performance improved as the backing condition became less conductive and more thermally resistive, as depicted in Table 6.

The aluminium backing condition gave the lowest tensile response among the three backing conditions. The measured tensile strengths ranged from 93.20 to 113.41 MPa, corresponding to joint efficiencies of 51.55% to 62.72%. The best result in this condition was 113.41 MPa with 62.72% joint efficiency. This comparatively low performance is consistent with the defective weld appearance seen in the same condition.

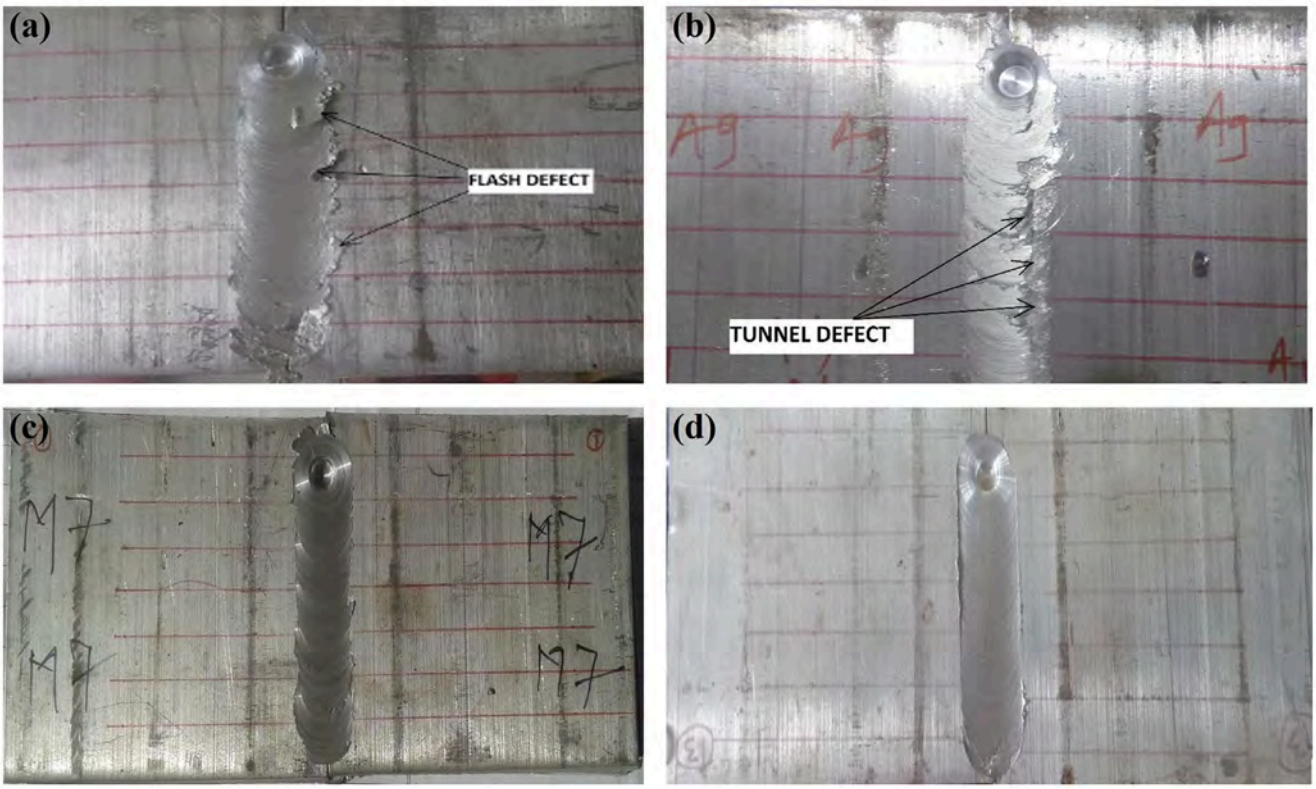

Figure 6: Weld appearance obtained under different backing conditions: (a,b) aluminium backing condition, (c) mild-steel backing condition, and (d) fly-ash-bed backing condition

Table 6. Tensile strength and joint efficiency under different backing conditions

Backing condition	Tensile strength range (MPa)	Maximum tensile strength (MPa)	Joint-efficiency range (%)	Maximum joint efficiency (%)
Aluminium	93.20–113.41	113.41	51.55–62.72	62.72
Mild steel	72.43–139.10	139.10	40.06–76.93	76.93
Fly ash	107.10–165.78	165.78	59.23–91.69	91.69

The mild-steel backing condition improved the tensile response substantially. The measured strength values ranged from 72.43 to 139.10 MPa, and joint efficiency varied from 40.06% to 76.93%. The best weld under these conditions reached 139.10 MPa, corresponding to 76.93% joint efficiency. The mild-steel condition, therefore, produced a clear improvement over the aluminium condition, which agrees with the smoother weld-bead morphology and lower defect severity.

The fly-ash backing condition produced the best overall mechanical performance. The measured tensile strength ranged from 107.10 to 165.78 MPa, while joint efficiency ranged from 59.23% to 91.69%. The highest value obtained in the entire study was 165.78 MPa, corresponding to 91.69% joint efficiency. The results further note that, in this condition, joint efficiency sometimes approached 90% of the base-metal strength, and the weld nugget surface was particularly fine. This confirms that the thermally insulating fly-ash bed provided the most favourable welding condition among the three cases examined.

3.3 Taguchi response analysis and ANOVA

The Taguchi single-response analysis in Table 7 showed that the relative importance of the process parameters changed with backing condition. For the aluminium condition, the ANOVA results revealed that welding speed was the most influential factor for tensile strength, contributing 60.31%, followed by tool rotational speed (17.86%) and tool geometry (16.5%). The corresponding prediction plot showed reasonable agreement between experimental and predicted tensile strength, with R^2 = 0.9469.

For the mild-steel condition, the dominant factor shifted from welding speed to tool rotational speed, which contributed 58.62% to the tensile-strength response. Welding speed contributed 32.26%, while tool geometry contributed 7.7%. The model showed strong adequacy, with R^2 = 0.9864, indicating close agreement between measured and predicted values.

Table 6. Tensile strength and joint efficiency under different backing conditions

Backing condition	Dominant parameter	Contribution (%)	Other contributions (%)	Predictive adequacy
Aluminium	Welding speed	60.31	Rotational speed: 17.86; Tool geometry: 16.5	$R^2 = 0.9469$
Mild steel	Rotational speed	58.62	Welding speed: 32.26; Tool geometry: 7.7	$R^2 = 0.9864$
Fly ash	Rotational speed	54.68	Welding speed: 22.0; Tool geometry: 23.0	$R^2 = 0.9979$

For the fly-ash condition, tool rotational speed again remained the dominant factor, with a contribution of 54.68%, while welding speed and tool geometry contributed 22.0% and 23.0%, respectively. The predictive relation for this condition gave the highest goodness of fit, with $R^2 = 0.9979$, indicating excellent agreement between experimental and predicted tensile strengths. This condition also yielded the highest joint efficiency and the most favourable weld appearance.

3.4 Hardness response under different backing conditions

The hardness results showed a trend opposite to the tensile-strength trend, as shown in Figure 7. In the aluminium condition, the hardness of the welded specimen was reported to be higher than that of the base metal at the measured locations. The results attribute this to a quenching effect caused by rapid heat extraction through the aluminium back plate, top plate, and side plates. It was also observed that hardness increased in the nugget zone and then decreased toward the advancing and retreating sides.

In the mild-steel condition, the hardness of the welded specimen also remained generally above the base metal, but the trend was more moderate. It was observed that the hardness at 4 mm thickness was nearly similar to that of the base metal and that, unlike the aluminium condition, no strong quenching effect existed because heat transfer through mild steel was only moderate. In this condition, the top and bottom regions tended to show relatively higher hardness than the interior levels.

In the fly-ash condition, the hardness profile was reported to remain close to the base-metal hardness. A clear gradient was observed from crown to root, with hardness being highest near the crown and decreasing downward; the root region sometimes showed hardness values even below the base metal. The results directly relate this behaviour to the thermal insulation of the fly-ash bed, which restricted heat loss from the bottom side and eliminated the quenching-like effect seen in the metallic backing conditions. Thus, although the fly-ash condition gave the highest tensile strength and joint efficiency, it did not give the highest hardness.

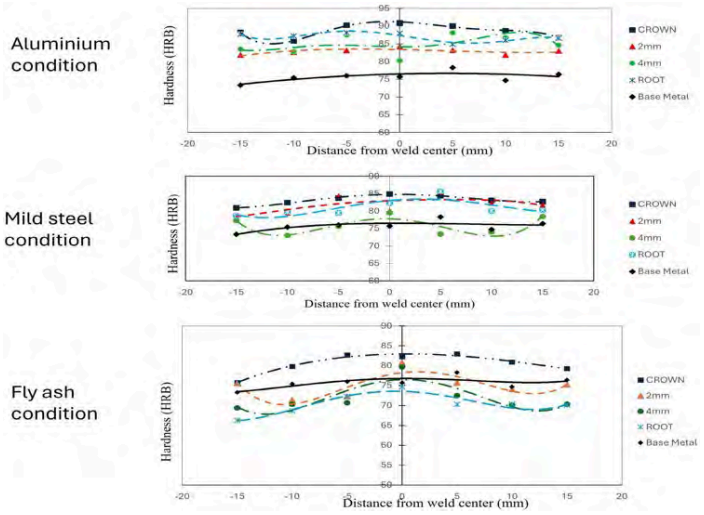

Figure 7. Hardness distributions under the three backing conditions: aluminium condition, mild-steel condition, and fly-ash condition

3.5 Fractography of tensile specimens

SEM fractography provided direct evidence of the failure mode under the different backing conditions, as shown in Figure 8. The base metal showed fine dimples with micro-void coalescence, which is characteristic of ductile fracture (Figure 8(a)). This base-metal morphology was used as the reference condition for comparison with the welded joints.

In the aluminium condition, the fracture surface showed tunnel defects, voids, featureless regions, and coarse dimples (Figure 8(b)). It was noted that a trans-granular fracture mode was present near the defect region, indicating a rough fracture surface with high crack-deflection angles. These features are fully consistent with the lower tensile performance measured in this condition.

In the mild-steel condition, the fractured tensile specimens showed fewer voids, fewer featureless regions, and fewer coarse dimples than those observed for the aluminium condition, as shown in Figure 8(c). Although the morphology was improved, it still did not reach the ductile appearance of the base metal or the fly-ash condition. The mild-steel condition, therefore, represents an intermediate fracture response between the highly conductive aluminium condition and the insulating fly-ash condition.

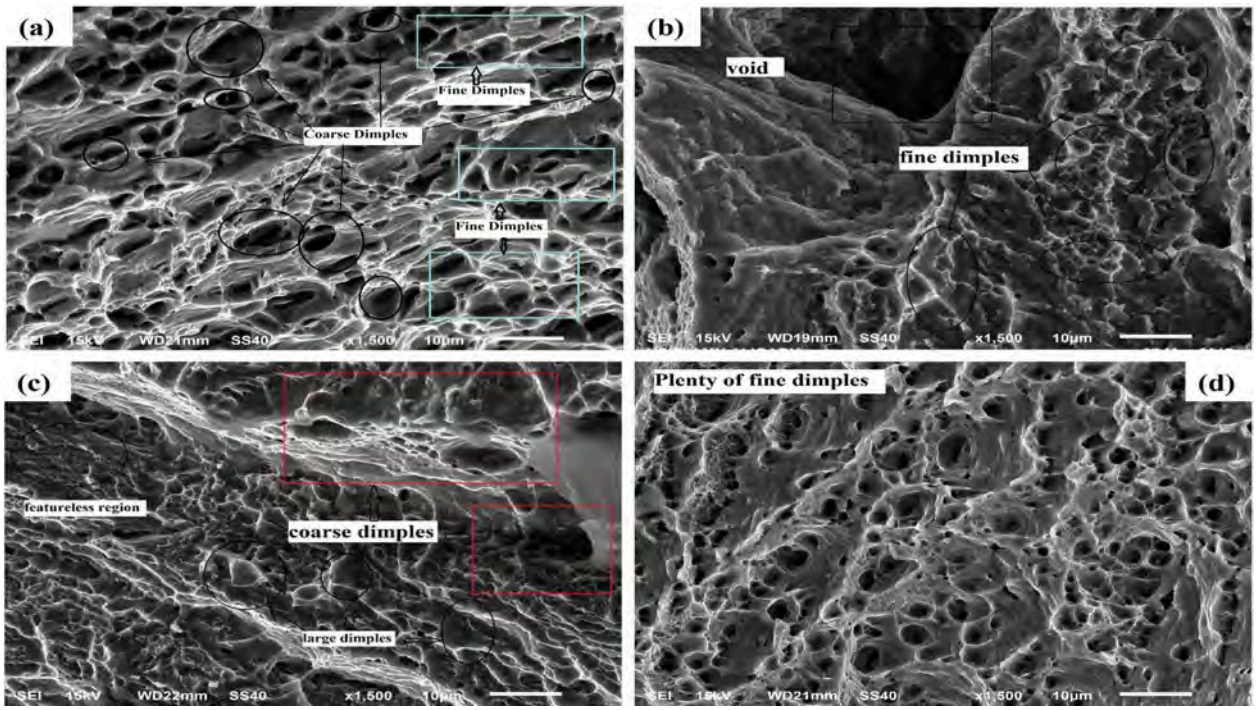

Figure 8. SEM fractography of tensile-tested specimens, (a) base metal, (b) aluminium backing condition, (c) mild-steel backing condition, and (d) fly-ash-bed backing condition

The most favourable fracture morphology was obtained in the fly-ash condition. The fractured surfaces were described as containing plenty of dimples with uniform sizes and depths, indicating typical ductile fracture, as depicted in Figure 8 (d). The dimples in the fly-ash condition were far more numerous than those in the aluminium and mild-steel conditions, and the fracture morphology was nearly similar to that of the base metal.

3.6 XRD analysis

XRD analysis was carried out on the base metal and on selected specimens from the three process conditions, as shown in Figure 9. The recorded patterns showed that there were no precipitates in the aluminium base material, which agrees with the EDS result indicating 100% aluminium.

More importantly, the XRD results showed that no foreign material was introduced during welding. This was particularly relevant for the fly-ash condition, because there was a possibility of fly-ash induction into the welded region. The XRD patterns of representative fly-ash specimens, such as F2 (Fly ash condition) and F5 (Fly ash condition), showed the same peaks as the other conditions, thereby confirming that fly ash was not introduced into the nugget zone.

4. Discussion

The present results show that the backing condition was not merely a supporting arrangement, but a governing thermal boundary condition that substantially altered weld formation, tensile response, hardness behaviour, and

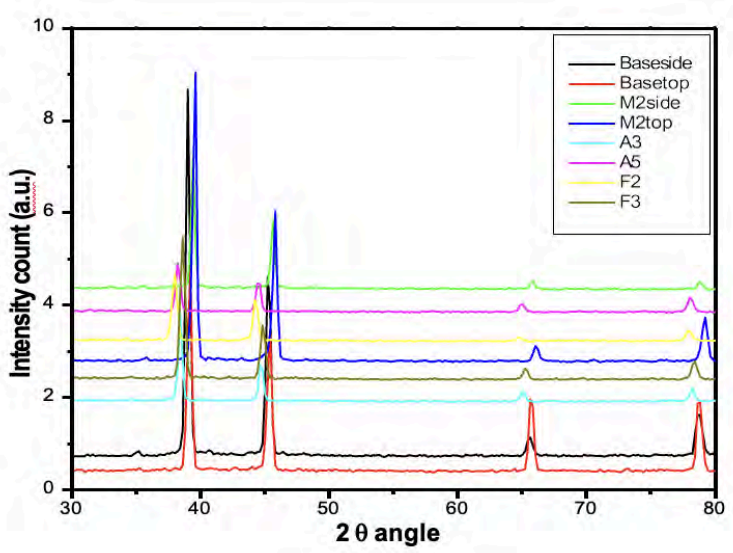

Figure 9: XRD patterns of the base metal and selected welded specimens from the aluminium, mild-steel, and fly-ash conditions

fracture morphology. In the present work, the change from aluminium backing to mild-steel backing and finally to the fly-ash bed progressively improved weld appearance and joint efficiency, with the fly-ash condition producing the highest tensile strength (165.78 MPa) and maximum joint efficiency (91.69%), whereas the aluminium condition gave the lowest efficiency and exhibited flash and tunnel-type defects. This trend indicates that the local heat extraction pathway beneath the weld played a decisive role in determining whether the material remained sufficiently plasticised for proper consolidation. Because the same Grade 310 tool was used in all experiments, the differences among the three cases are attributed mainly to backing-controlled heat extraction rather than to changes in tool thermal response; however, the relatively low thermal conductivity of the stainless-steel tool likely contributed to local heat retention in all runs (Das et al., 2024). Similar conclusions have been reported in recent backing-plate studies, where backing selection modified local heat transfer, weld temperature, cooling rate, and final mechanical performance; low-conductivity or thermally favourable backing conditions tended to improve heat utilisation, while highly conductive support conditions increased the risk of under-heated weld roots or reduced flow stability (Mondal et al., 2024; Park et al., 2020; Verma et al., 2025).

The comparatively poor performance of the aluminium backing condition can be explained by excessive heat extraction from the weld zone. Because aluminium possesses the highest thermal conductivity among the three selected conditions, the heat generated by friction and deformation was more rapidly dissipated into the bottom, top, and side supports, narrowing the available process window for stable plasticisation. The findings' interpretation is fully consistent with this mechanism: under the aluminium condition, insufficient heat remained available for proper mixing, and the fracture surfaces showed tunnel defects, voids, featureless regions, and coarse dimples near the defect region.

Such behaviour corresponds closely to the literature on backing-plate effects, where rapid heat loss through highly conductive backing materials has been associated with insufficient root-side softening, unstable flow, and defect formation. Park et al. (2020), for example, reported that higher heat-loss backing conditions in micro-FSW promoted inferior joint formation compared with more thermally resistant conditions, while Verma et al. (2025) further showed that backing diffusivity directly affects thermal symmetry and flow behaviour in dissimilar aluminium μFSW.

The superiority of the fly-ash condition can be interpreted as the opposite thermal case. The fly-ash bed acted as a thermal insulator, restricting heat loss from the lower surface and thereby allowing a larger volume of softened material to remain available around the pin and beneath the shoulder. This would favour material transport from the advancing side to the retreating side and, more importantly, along the thickness direction, thereby improving void closure and weld continuity. The results explicitly link the higher fly-ash joint efficiency to sufficient heat being retained in the weld zone, very fine plasticisation, proper mixing, and a smooth, mirror-like, defect-free weld surface. Recent studies support this general interpretation. Mondal et al. (2024) showed that the backing plate condition altered the thermal cycle and thereby changed the resulting strength and microstructure in the friction stir-welded Al-Li alloy. Das et al. (2024) likewise demonstrated that thermal boundary conditions and cooling strategy in thick aluminium FSW influence joint strength and grain-size distribution across the weld thickness. Verma et al. (2025) further confirmed that strategic control of backing diffusivity can improve heat utilisation and velocity-field symmetry, leading to better mechanical response. Within this framework, the fly-ash bed in the present study can be understood as an effective insulating thermal boundary that reduced heat drainage and enhanced consolidation quality.

The Taguchi and ANOVA results also become more meaningful when viewed through this thermal-boundary perspective. Under the aluminium backing condition, welding speed was the dominant factor, whereas under mild steel and fly ash, rotational speed became dominant. This shift suggests that when heat loss is severe, residence time becomes the most critical issue because the tool must remain long enough at a given location to develop the plasticised volume needed for sound bonding. Once heat dissipation is moderated, as in mild steel and especially in fly ash, the process becomes more sensitive to the rate of heat generation and stirring action, which are more directly governed by rotational speed. Recent optimisation studies on AA6061 and related aluminium systems support this interpretation. Yacout et al. (2025) found that rotational speed and tool profile were among the most influential parameters for ultimate tensile strength in AA6061-T6 FSW, while Wahjudi et al. (2024) showed that a Taguchi-based framework could effectively link tool configuration to mechanical response and fracture characteristics in AA6061-T651 joints. These reports reinforce the conclusion that parameter significance in FSW is not fixed, but depends on the surrounding thermal and mechanical boundary conditions.

An important outcome of the present work is that hardness did not follow the same ranking as tensile strength. The aluminium condition produced the highest hardness, whereas the fly-ash condition produced hardness values close to the base metal, despite giving the best tensile performance. This difference is significant because it shows that the tensile response in the present joints was governed more strongly by consolidation quality and defect suppression than by hardness increase alone. This attributes the higher hardness in the aluminium condition to a quenching-like effect caused by rapid heat removal through the metallic support system, whereas in the fly-ash condition, the absence of strong heat extraction eliminated this quenching effect and produced a crown-to-root decrease in hardness. Recent literature supports the broader principle that thermal boundary conditions can substantially reshape hardness distributions by altering the cooling rate and local metallurgical response. Mondal et al. (2024) showed that backing condition changes the thermal cycle and therefore the resulting property balance in FSWed aluminium, while Das et al. (2024) reported that quenching and cooling rate strongly affect local mechanical response across the weld thickness.

In AA6061 specifically, Zhou et al. (2024) further demonstrated that thermal history influences precipitate evolution and joint efficiency after welding, confirming that hardness variation in 6xxx alloys is highly sensitive to heat-treatment-like effects. Even though the present material was pure aluminium, the same principle applies: hardness reflects local thermal history, whereas tensile strength in defective welds may be dominated by macroscopic integrity rather than local hardness alone.

The fractographic evidence strongly supports this distinction between hardness-controlled and defect-controlled behaviour. The base metal exhibited fine dimples with micro-void coalescence, consistent with ductile fracture. In the aluminium condition, however, the fracture surfaces contained tunnel defects, voids, featureless regions, and coarse dimples, indicating mixed-mode failure initiated or accelerated by poor consolidation. The mild-steel condition showed an intermediate response with fewer severe defect features, whereas the fly-ash condition displayed abundant, fine, and deep dimples and a fracture appearance close to that of the base metal. This progression from mixed-mode, defect-assisted fracture to a more uniformly ductile dimple rupture directly mirrors the progression in joint efficiency. Recent AA6061 studies similarly use fractography to interpret weld quality and failure mode. Wahjudi et al. (2024) linked fracture characteristics to tool-design-induced changes in mechanical response, while Yacout et al. (2025) showed that systematically optimised FSW conditions can produce defect-free joints with predictable hardness and strength behaviour. Accordingly, the fractography in the present work is not merely descriptive; it provides direct evidence that the fly-ash condition improved the actual integrity of the welded region rather than only modifying its hardness response.

The XRD observations provide an additional level of confidence in interpreting the fly-ash condition. Because fly ash was used as an unconventional insulating medium, a reasonable concern was whether particles from the bed might be mechanically introduced into the weld nugget. The XRD results showed no additional peaks, and the fly-ash welds exhibited the same peak positions as the other conditions, indicating that no detectable foreign material was introduced into the nugget zone.

This finding is important because it confirms that the beneficial effect of the fly-ash backing condition arose from thermal boundary control, not from chemical contamination or reinforcement. It also supports the practical attractiveness of the approach: the fly-ash bed functioned as a low-cost insulating process condition capable of improving joint efficiency without causing detectable phase contamination. Taken together, the present results indicate that backing condition should be treated as an active design variable in FSW parameter optimisation, particularly when the work is performed on conventional milling-based systems where process stability is more sensitive to fixture and heat-loss conditions than on dedicated industrial FSW platforms.

5. Conclusion

This study examined the friction stir welding of 6-mm pure aluminium under three different backing conditions, namely aluminium, mild steel, and fly ash, using a Taguchi L9 design to optimise the principal welding parameters. On the basis of the experimental results, the following conclusions can be drawn.

The developed fixture was effective for carrying out friction stir welding on a conventional vertical milling machine. It provided stable clamping, reduced setup difficulty, and allowed the welding trials to be performed under controlled and repeatable conditions. The backing condition had a pronounced influence on weld appearance, tensile behaviour, joint efficiency, hardness response, and fracture morphology. Among the three conditions studied, the fly-ash backing condition provided the most favourable overall weld performance.

The aluminium backing condition produced the lowest tensile performance, with tensile strength in the range of 93.20-113.41 MPa and joint efficiency in the range of 51.55-62.72%. The mild-steel backing condition improved joint performance compared with aluminium backing, producing tensile strength in the range of

72.43-139.10 MPa and joint efficiency in the range of 40.06-76.93%. The fly-ash backing condition gave the best overall performance, producing tensile strength in the range of 107.10-165.78 MPa and joint efficiency in the range of 59.23-91.69%.

The hardness profile did not follow the same ranking as tensile strength. The maximum hardness was observed in the aluminium condition, where hardness remained above the base-metal value, while the fly-ash condition produced hardness values closer to the base metal. The mild-steel condition showed intermediate hardness behaviour.

The fracture morphology strongly supported the tensile results. Welds produced in the fly-ash condition exhibited fracture surfaces similar to the base metal, with typical ductile fracture characterised by plenty of fine and deep dimples, whereas welds produced in the aluminium and mild-steel conditions showed mixed-mode fracture.

The XRD analysis showed that no foreign material was introduced during welding, including under the fly-ash backing condition. This confirms that the beneficial effect of the fly-ash condition arose from its thermal-insulation role rather than from any foreign-material incorporation into the weld zone.

Overall, the results show that backing condition is an important optimisation variable in friction stir welding of pure aluminium and that fly ash can serve as an effective low-cost insulating backing medium. Future work may extend this concept to aluminium alloys, different plate thicknesses, and closed-section products such as pipes and hollow profiles.

Data Availability

Data sets generated during the current study are available from the corresponding authors on reasonable request.

Declaration of Competing Interest

The authors declare that they have no known competing financial interests or personal relationships that could have appeared to influence the work reported in this paper.

Acknowledgements

The authors would like to acknowledge the Daou (Shaoxing) Technology Co., Ltd, Shaoxing City, Zhejiang Province, China, for providing the necessary facilities and resources for this research.

References

Abdelhady, S. S., Elbadawi, R. E., & Zoalfakar, S. H. (2024). Multi-objective optimization of FSW variables on joint properties of AA5754 aluminum alloy using Taguchi approach and grey relational analysis. *The International Journal of Advanced Manufacturing Technology*, *130*(9), 4235–4250.

Abdollahzadeh, A., Bagheri, B., Abassi, M., Kokabi, A. H., & Moghaddam, A. O. (2021). Comparison of the weldability of AA6061-T6 joint under different friction stir welding conditions. *Journal of Materials Engineering and Performance*, *30*(2), 1110–1127.

Acharya, U., Choudhury, S., Sethi, D., Akinlabi, E., & Roy, B. S. (2024). Enhancing joint performance in friction stir welding through tailored double-butt-lap geometry. *Welding in the World*, *68*(5), 1089–1101.

Ahmed, S., Rahman, R. A. ur, Awan, A., Ahmad, S., Akram, W., Amjad, M., Yahya, M. Y., & Rahimian Koloor, S. S. (2022).

Optimization of process parameters in friction stir welding of aluminum 5451 in marine applications. *Journal of Marine Science and Engineering*, *10*(10), 1539. https://doi.org/10.3390/jmse10101539

Al-Allaq, A. H., Maniscalco, J., Bhukya, S. N., Wu, Z., & Elmustafa, A. (2024). Parametric optimization of friction stir welding of AA6061-T6 samples using the copper donor stir-assisted material method. *Metals*, *14*(5), 536.

Ambrosio, D., Morisada, Y., Ushioda, K., & Fujii, H. (2024). Extremely thin intermetallic layer in dissimilar AA6061-T6 and mild steel friction stir lap welding using a hemispherical tool. *Scientific Reports*, *14*(1), 1718.

Amini, C., Jerez-Mesa, R., Travieso-Rodriguez, J. A., Mousavi, H., Lluma-Fuentes, J., Zandi, M. D., & Hassanifard, S. (2022). Ball burnishing of friction stir welded aluminum alloy 2024-T3: experimental and numerical studies. *Metals*, *12*(9), 1422.

Asmare, A., Al-Sabur, R., & Messele, E. (2020). Experimental investigation of friction stir welding on 6061-t6 aluminum alloy using taguchi-based gra. *Metals*, *10*(11), 1480.

Bharti, S., Kumar, S., Singh, I., Kumar, D., Bhurat, S. S., Abdullah, M. R., & Rahimian Koloor, S. S. (2023). A review of recent developments in friction stir welding for various industrial applications. *Journal of Marine Science and Engineering*, *12*(1), 71.

Choi, J.-W., Hino, R., Ushioda, K., Fujii, H., & Lee, S.-J. (2025). Critical Review of Solid-State Welding for Al Alloys with High Joint Efficiency: Friction Stir Welding (FSW) vs. Linear Friction Welding (LFW). *Metals and Materials International*, 1–25.

Clark, A., & Ragai, I. (2025). Adaptive Torque Control for Process Optimization in Friction Stir Welding of Aluminum 6061-T6 Using a Horizontal 5-Axis CNC Machine. *Journal Of Manufacturing And Materials Processing*, *9*(7), 232.

Das, H., Reza-E-Rabby, M., Whalen, S. A., Upadhyay, P., & Grant, G. J. (2024). Impact of backing plate and thermal boundary conditions for high-speed friction stir welding of 25-mm thick aluminum alloy 7175-T79. *International Journal of Precision Engineering and Manufacturing-Green Technology*, *11*(6), 1757–1767.

Feddal, I., Chairi, M., & Di Bella, G. (2025). Analysis of friction stir welding of aluminum alloys. *Metals*, *15*(5), 532.

Habba, M. I. A., & Ahmed, M. M. Z. (2025). Friction stir welding of dissimilar aluminum and copper alloys: A review of strategies for enhancing joint quality. *Journal of Advanced Joining Processes*, *11*, 100293.

Heidarzadeh, A., Mironov, S., Kaibyshev, R., Çam, G., Simar, A., Gerlich, A., Khodabakhshi, F., Mostafaei, A., Field, D. P., Robson, J. D., Deschamps, A., & Withers, P. J. (2021). Friction stir welding/processing of metals and alloys: A comprehensive review on microstructural evolution. *Progress in Materials Science*, *117*, 100752. https://doi.org/https://doi.org/10.1016/j.pmatsci.2020.100752

Isa, M. S. M., Moghadasi, K., Ariffin, M. A., Raja, S., bin Muhamad, M. R., Yusof, F., Jamaludin, M. F., bin Yusoff, N., & bin Ab Karim, M. S. (2021). Recent research progress in friction stir welding of aluminium and copper dissimilar joint: a review. *Journal of Materials Research and Technology*, *15*, 2735–2780.

Kubit, A., Trzepieciński, T., Kluz, R., Ochałek, K., & Slota, J. (2022). Multi-criteria optimisation of friction stir welding parameters for EN AW-2024-T3 aluminium alloy joints. *Materials*, *15*(15), 5428.

Lunetto, V., De Maddis, M., Lombardi, F., & Russo Spena, P. (2025). A review of friction stir welding of industrial alloys: tool design and process parameters. *Journal of Manufacturing and Materials Processing*, *9*(2), 36.

Manjunatha, C., N, S. T., V, M. S., Shivanayak, L., Panditharadhya, B. J., Prasad, C. D., Masum, H., Kumar, C. H., & Aden, A. A. (2025). Experimental investigation and optimization of friction stir welding parameters to manufacture AA6061-B4C composite material using design of experiments. *Journal of Materials Science: Materials in Engineering*, *20*(1), 117.

Mohd Jamil, M. Z., Mohd Isa, M. S., Raja, S., bin Muhamad, M. R., Yusof, F., Hasnan, H. K., Jamaludin, M. F., Brytan, Z., Liu, H., Suga, T., Morisada, Y., & Fujii, H. (2024). Friction Stir Alloying AZ61 Magnesium Alloy and Mild Steel with Zn-CNT Additive. *Transactions of the Indian Institute of Metals*, *77*(2), 435–443. https://doi.org/10.1007/s12666-023-03124-8

Mondal, B., Sinha, S., Reed, J., Lee, H.-S., Doherty, K. J., & Mishra, R. S. (2024). Effect of backing plate on microstructure and properties of friction stir welded 2195-O alloy. *Scripta Materialia*, *241*, 115899.

Myśliwiec, P., Kubit, A., & Szawara, P. (2024). Optimization of 2024-T3 aluminum alloy friction stir welding using random forest, XGBoost, and MLP machine learning techniques.
Materials, *17*(7), 1452.

Park, S., Joo, Y., & Kang, M. (2020). Effect of backing plate materials in micro-friction stir butt welding of dissimilar AA6061-T6 and AA5052-H32 aluminum alloys. *Metals*, *10*(7), 933.

Raja, S., Hasan, F., Ansari, A. H., & Ansari, H. (2016). *Effect of Friction Stir Welding on the Hardness of Al-6061 T6 aluminium alloy*.

Raja, S., Manikumar, R., Benruben, R., & Ragunathan, S. (2021). Effect of backing plate on strength and microstructural characteristics of friction stir welded AA2014-T6 aluminium alloy joints. *Materials Today: Proceedings*, *45*, 895–899.

Raja, S., Muhamad, M. R., Jamaludin, M. F., & Yusof, F. (2020). A review on nanomaterials reinforcement in friction stir welding. *Journal of Materials Research and Technology*, *9*(6), 16459–16487. https://doi.org/https://doi.org/10.1016/j.jmrt.2020.11.072

Raja, S., Muhamad, M. R., Yusof, F., Jamaludin, M. F., Suga, T., Liu, H., Morisada, Y., & Fujii, H. (2022). Friction stir alloying of AZ61 and mild steel with Al-CNT additive. *Science and Technology of Welding and Joining*, *27*(7), 533–540. https://doi.org/10.1080/13621718.2022.2080449

Raja, S., Yusof, F., Muhamad, M. R., Mohd Mansor, M. S., Juri, A., Wu, B., Jamaludin, M. F., Ansari, N., & Ren, J. (2024). Formation and influencing mechanism of the intermetallic compound in the friction stir welding of immiscible AZ31 and SPHC steel using aluminium powder as an additive. *Journal of Materials Research and Technology*, *30*, 9102–9114. https://doi.org/https://doi.org/10.1016/j.jmrt.2024.05.249

Soto-Diaz, R., Vasquez-Carbonell, M., & Escorcia-Gutierrez, J. (2025). A review of artificial intelligence techniques for optimizing friction stir welding processes and predicting mechanical properties. *Engineering Science and Technology, an International Journal*, *62*, 101949.

Tinguery, K. M. S., Rahem, A., Nadeau, F., & Fafard, M. (2023). Friction stir welding parameters development of AA6061-T6 extruded alloy using a bobbin tool. *Engineering Proceedings*, *43*(1), 50.

Tiwan, Ilman, M. N., Kusmono, & Sehono. (2023). Microstructure and mechanical performance of dissimilar friction stir spot welded AA2024-O/AA6061-T6 sheets: Effects of tool rotation speed and pin geometry. *International Journal of Lightweight Materials and Manufacture*, *6*(1), 1–14. https://doi.org/https://doi.org/10.1016/j.ijlmm.2022.07.004

Verma, M., Saha, P., & Singh, P. K. (2025). Optimizing heat utilization in dissimilar micro-friction stir welding of AA 2024-T3/AA 6061-T6 using dual backing plate: Impact on local microstructure, mechanical, and corrosion performance. *Journal of Manufacturing Processes*, *149*, 98–115.

Wahjudi, A., Pramono, A. S., & Batan, I. M. L. (2024). A study of concave shoulder angle on the mechanical properties and fractography of friction stir welded AA6061-T651 joints. *Journal of Materials Research and Technology*, *28*, 78–86.

Yacout, G. G., Shash, A. Y., Hegazi, H. A., & El-Sherbiny, M. G. (2025). Comparative experimental and statistical study of conventional and bobbin tool friction stir welding of AA6061-T6 aluminum alloy. *Journal of Engineering and Applied Scienc*e, 72(1), 255.

Yamani, S. M., Raja, S., bin Ariffin, M. A., Mohd Isa, M. S., Muhamad, M. R., Jamaludin, M. F., Yusof, F., & bin Ahmad Hairuddin, M. K. F. (2022). Effects of Preheating on Microstructural and Mechanical Properties of Friction Stir Welded Thin Low Carbon Steel Joints. *Journal of Engineering Materials and Technology,* 145(2). https://doi.org/10.1115/1.4055909

Zhou, D., Xia, Y., Gao, Z., Bai, L., & Hu, W. (2024). Effect of precipitate evolution on galvanic corrosion behavior of friction stir welded AA6061-T6 joint after post-weld aging. *Materials Today Communications,* 41, 110764.